



Understanding Fuel Magnetization and Mix Using Secondary Nuclear Reactions in Magneto-Inertial Fusion

P. F. Schmit, P. F. Knapp, S. B. Hansen, M. R. Gomez, K. D. Hahn, D. B. Sinars, K. J. Peterson, S. A. Slutz, A. B. Sefkow, T. J. Awe, E. Harding, C. A. Jennings, G. A. Chandler, G. W. Cooper, M. E. Cuneo, M. Geissel, A. J. Harvey-Thompson, M. C. Herrmann, M. H. Hess, O. Johns, D. C. Lamppa, M. R. Martin, R. D. McBride, J. L. Porter, G. K. Robertson, G. A. Rochau, D. C. Rovang, C. L. Ruiz, M. E. Savage, I. C. Smith, W. A. Stygar, and R. A. Vesey

Sandia National Laboratories, P.O. Box 5800, Albuquerque, New Mexico 87185-1186, USA

(Received 18 June 2014; published 6 October 2014)

Magnetizing the fuel in inertial confinement fusion relaxes ignition requirements by reducing thermal conductivity and changing the physics of burn product confinement. Diagnosing the level of fuel magnetization during burn is critical to understanding target performance in magneto-inertial fusion (MIF) implosions. In pure deuterium fusion plasma, 1.01 MeV tritons are emitted during deuterium-deuterium fusion and can undergo secondary deuterium-tritium reactions before exiting the fuel. Increasing the fuel magnetization elongates the path lengths through the fuel of some of the tritons, enhancing their probability of reaction. Based on this feature, a method to diagnose fuel magnetization using the ratio of overall deuterium-tritium to deuterium-deuterium neutron yields is developed. Analysis of anisotropies in the secondary neutron energy spectra further constrain the measurement. Secondary reactions also are shown to provide an upper bound for the volumetric fuel-pusher mix in MIF. The analysis is applied to recent MIF experiments [M. R. Gomez *et al.*, *Phys. Rev. Lett.* 113, 155003 (2014)] on the Z Pulsed Power Facility, indicating that significant magnetic confinement of charged burn products was achieved and suggesting a relatively low-mix environment. Both of these are essential features of future ignition-scale MIF designs.

DOI: [10.1103/PhysRevLett.113.155004](https://doi.org/10.1103/PhysRevLett.113.155004)

PACS numbers: 52.58.Lq, 52.55.Pi, 52.65.Pp, 52.70.Nc

Introduction.—Magneto-inertial fusion (MIF) offers some key advantages over traditional inertial confinement fusion (ICF). In MIF, fuel magnetization relaxes the extreme pressure requirements characteristic of traditional ICF and enhances thermal insulation of the hot fuel from the colder pusher [1–9]. We consider paradigmatically the radial compression of a long, thin cylinder of fuel magnetized with a uniform, axial field prior to compression [10–16]. At stagnation, the compressed magnetic flux redirects charged burn products axially, increasing the effective fuel areal density from ρR to ρZ , where ρ is the fuel mass density, R is the fuel radius, Z is the fuel length, and $A \equiv Z/R \gg 1$ is the aspect ratio.

Sandia National Laboratories has fielded the first integrated experiments investigating Magnetized Liner Inertial Fusion (MagLIF) [13–16], which involves direct compression of magnetized, preheated deuterium fuel by a solid metal (beryllium) liner, imploded on the 26 MA, 100 ns Z Pulsed Power Facility [17]. The imploding cylindrical liner compresses a preseeded axial magnetic field, B_0 (≈ 10 T in the first experiments), to high amplitude at stagnation, B , where perfect flux conservation would imply $B = B_0(R_0/R)^2$, and the initial fuel radius is $R_0 = 2.325$ mm. However, detailed simulations suggest that multiple effects (e.g., resistive losses, Nernst effect) can lead to leakage of magnetic flux out of the hot fuel [13,16]. Thus, diagnosing the efficacy of flux compression

in experiments is critical for understanding target performance and the viability of the concept.

Improved performance of laser-driven ICF targets via fuel premagnetization was realized for the first time only very recently [18–20]. Unlike these experiments, MIF concepts like MagLIF rely critically on magnetization for functionality, not simply to improve performance. External charged-particle probing methods like proton deflectometry [18,19,21–23] cannot be used to diagnose fuel magnetization in MagLIF, since the target is enshrouded by a large volume of strong ($\gtrsim 50$ MG) azimuthal fields generated by the pulsed power driver. Then, the essential diagnostic signature of fuel magnetization must arise from signals produced within the burning fuel itself.

In this Letter, we show that the level of fuel magnetization during burn in MIF can be inferred from secondary fusion reactions. In pure deuterium fuel, deuterium-deuterium (DD) fusion reactions produce roughly equal numbers of 1.01 MeV tritons and 2.45 MeV neutrons. Some tritons undergo secondary fusion reactions with the deuterium fuel, producing 14.1 MeV neutrons. We use the magnetic confinement and stopping of secondary tritons in the fuel as a probe of the fuel magnetization and mix. The first integrated MagLIF experiments have produced significant DD fusion yields [$Y_{DD} = O(10^{12})$ DD neutrons] and remarkable secondary deuterium-tritium (DT) yields [$Y_{DT} = O(10^{10})$ DT neutrons], with the best-performing

shot producing $Y_{\text{DT}}/Y_{\text{DD}} \equiv \bar{Y} = (2.8 \pm 1.5) \times 10^{-2}$ [17]. We show that these DT yields are a consequence of fuel magnetization, which dramatically elongates the triton path lengths through the fuel, increasing their probability of reaction. Analysis of \bar{Y} and the anisotropies in the secondary neutron energy spectra provide two relatively independent methods to obtain estimates of the volume-averaged magnetization, leading unambiguously to the conclusion that the first MagLIF experiments achieved significant fuel magnetization during burn. In addition, secondary yields are known to correlate with mix in unmagnetized ICF [24,25]. We show that \bar{Y} can constrain the amount of volumetric mix during burn in MIF, providing evidence that MagLIF experiments also achieved a relatively low-mix hot spot.

Understanding fuel magnetization with the DT:DD yield ratio.—We focus here on large aspect ratio ($A \gg 1$), uniformly magnetized cylinders of fusion fuel to permit a direct comparison with experimental MagLIF results [17]. The probability per unit path length for a triton i within a deuterium plasma to undergo DT fusion is $P_i[\mathbf{v}_i, \mathbf{x}] = n_d(\mathbf{x}) \int d\mathbf{v} (|\mathbf{v} - \mathbf{v}_i|/v_i) f_d(\mathbf{x}, \mathbf{v}) \sigma_{\text{DT}}(|\mathbf{v} - \mathbf{v}_i|) \equiv n_d \tilde{\sigma}[\mathbf{v}_i, \mathbf{x}]$, where n_d is the local deuterium number density, f_d is the normalized distribution of deuteron velocities (i.e., $\int d\mathbf{v} f_d = 1$), \mathbf{v}_i is the triton velocity, and σ_{DT} is the total DT reaction cross section [26]. The mean cross section $\tilde{\sigma}$ is a functional of the triton speed, $v_i(\mathbf{x}) = |\mathbf{v}_i|$, when f_d is isotropic, which we assume here. Simulated tritons act as *quasiparticles*, each carrying the initial statistical weight, w_i , of many identical tritons, which diminishes along each trajectory as reactions occur. For an ensemble of N quasiparticles, $Y_{\text{DD}} \propto \sum_i^N w_i$, and $Y_{\text{DT}} \propto \sum_i^N w_i \mathcal{R}_i$, where \mathcal{R}_i is the reacted fraction of each quasiparticle. Setting $w_i = 1$, and noting that $d\mathcal{R}_i/ds = [1 - \mathcal{R}_i(s)]P_i[v_i(s), s]$, with $s = s(\mathbf{x})$ the length along each trajectory, we find

$$\bar{Y} = \frac{1}{N} \sum_i^N \int_0^{\ell_i} [1 - \mathcal{R}_i(s)] n_d(s) \tilde{\sigma}[v_i(s), s] ds \equiv \langle \mathcal{R} \rangle. \quad (1)$$

ℓ_i are the path lengths, or *ranges*, between the triton birth locations and the points at which they leave the fuel or thermalize. Angled brackets $\langle \rangle$ henceforth represent the ensemble average over all tritons.

In the case of uniform fuel ($n_d = n_0$), weak collisionality ($v_i \approx v_0$), and $\mathcal{R}_i \ll 1$, one finds that $\bar{Y} \propto \rho \langle \ell \rangle$. In this *collisionally thin* limit, \bar{Y} scales linearly with the average fuel areal density sampled by the tritons. As the fuel becomes more dense, and possibly inhomogeneous, a more complex, but still well defined, relationship exists between $\langle \rho \ell \rangle$ and \bar{Y} . Correspondingly, methods to estimate the fuel areal density in *unmagnetized* implosions using \bar{Y} are now well established [27–31].

In MIF, $\langle \ell \rangle$ varies strongly with magnetization, implying that with some knowledge of the burn-averaged fuel

density, temperature, and dimensions, the burn-averaged magnetization can be estimated from \bar{Y} . This concept is explored using two physics codes to model the transport and reactivity of secondary tritons in magnetized, cylindrical deuterium cavities. The first code [32] employs a kinetic, Landau-Fokker-Planck formalism to calculate triton scattering off of fuel ions and electrons. The second code [33] computes \bar{Y} and neutron energy spectra using the triton trajectories calculated in the first code. Tritons are “lost” when they escape the fuel, when their energy thermalizes to the fuel temperature, or when 2 ns have elapsed—a number based on experimental estimates of burn time [17]. Both the axial magnetic field and fuel are treated as uniform and stationary over the triton lifetimes [$O(0.5 \text{ ns})$]. The assumption of stationary, homogeneous fuel allows the dominant scalings of \bar{Y} to be identified, yet reasonable agreement is found when comparing to time- and volume-averaged results from radiation-magnetohydrodynamic and kinetic simulations [16] of the recent experiments [17].

In this section, each simulated cylindrical plasma cavity is defined by a pure deuterium mass density (ρ_d), temperature (T), axial magnetic field strength (B), fuel radius (R), and aspect ratio (A). Fuel electrons and ions are Maxwellian with equal temperatures, $T_i = T_e = 3.1 \text{ keV}$, based on x-ray spectroscopy of continuum electron emission from the highest yield MagLIF shot [17]. (Small differences in the T_i inferred from neutron time-of-flight data compared to T_e have a negligible impact on the present calculations.) The cylinder dimensions— $R = 50 \mu\text{m}$, and $A = 80$ —are chosen based on emission imaging and spectroscopy. The density, $\rho_d = 0.4 \text{ g/cm}^3$, is chosen based on DD neutron and x-ray emission histories, leading to $\rho_d R = 2 \text{ mg/cm}^2$. Tritons are born isotropically and uniformly within the fuel, with a spread in energies about the mean proportional to $T^{1/2}$ [34].

Figure 1(a) shows $\bar{Y}(BR)$ for several values of $\rho_d R$, including collisionally thin ($\rho_d R = 0.1 \text{ mg/cm}^2$) and collisionally thick ($\rho_d R = 200 \text{ mg/cm}^2$) limiting cases, where very little and nearly complete triton slowing occurs, respectively. In the collisionally thick case, the fuel stops tritons effectively independent of the strength of B . At lower $\rho_d R$, however, \bar{Y} varies significantly with B . The similar threshold behavior as the magnetic-field–radius product (BR) increases shared by the curves at different $\rho_d R$ indicates that the increase in \bar{Y} is primarily a geometric consequence of the diminishing triton Larmor radius relative to the fuel radius ($R/r_{L,i} \propto BR$). Reference [10] reports qualitatively similar trends in the α -particle energy deposition fraction for cylindrical, magnetized DT fuel.

In fact, an expression for the fraction of radially confined (*trapped*) tritons, F_t , born isotropically in a large aspect ratio cylinder and averaged over the fuel volume, can be written solely as a function of BR , which we state here (the derivation is left for a future publication):

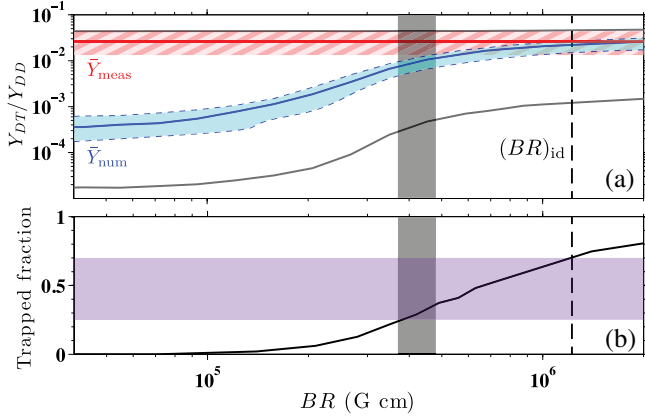


FIG. 1 (color online). (a) Calculated DT:DD neutron yield ratio \bar{Y}_{num} versus the magnetic-field-radius product (BR) for $\rho_d R = 2$ mg/cm² (estimated MagLIF conditions [17], central, solid blue line), and collisionally thin ($\rho_d R = 0.1$ mg/cm², lower gray line) and collisionally thick ($\rho_d R = 200$ mg/cm², upper gray line) limits, for deuterium fuel with $R = 50$ μ m, $A = 80$, and $T = 3.1$ keV. $(BR)_{id}$ corresponds to BR obtained by perfect flux compression (vertical dashed line). Red line and red, diagonally hatched area denote experimentally observed $\bar{Y}_{meas} = (2.8 \pm 1.5) \times 10^{-2}$ [17]. Blue region denotes the confidence interval for \bar{Y}_{num} , reflecting model output sensitivity to variations of the inputs based on experimental measurement uncertainties. Intersection of red and blue regions satisfying $BR \lesssim (BR)_{id}$ represents most likely experimental conditions. Vertical gray region indicates BR range estimated from neutron spectra (Fig. 2). (b) Volume-averaged trapped fraction versus BR for 1.01 MeV tritons. Purple shaded area indicates trapped fraction range inferred from \bar{Y} and neutron spectra.

$$F_t = 1 - \frac{2}{\pi(\alpha BR)^2} \int_0^{\alpha BR} d\tilde{r} \tilde{r} \left(\pi \mu_2(\tilde{r}) - \int_{\mu_1}^{\mu_2} d\mu \cos^{-1} \left[\frac{\tilde{r}^2 - (\alpha BR)^2 + 2\alpha BR \sqrt{1 - \mu^2}}{2\tilde{r} \sqrt{1 - \mu^2}} \right] \right). \quad (2)$$

Here, $\alpha = (Br_{L,t})^{-1}$, $\mu_{1,2} = \sqrt{x_{1,2} \Theta(x_{1,2})}$, $\Theta(x)$ is the step function, and $x_{1,2} = 1 - (\alpha BR \pm \tilde{r})^2/4$. Figure 1(b) shows Eq. (2) for 1.01 MeV tritons, indicating that when $BR > 10^5$ G cm, a significant population of tritons is confined by the magnetic field. Magnetically trapped tritons sample a fuel areal density scaling like $\rho_d Z$, while untrapped tritons sample an areal density scaling like $\rho_d R$. One can estimate $\bar{Y} \approx F_t \bar{Y}_t + (1 - F_t) \bar{Y}_u$, where \bar{Y}_t and \bar{Y}_u are the trapped and untrapped triton average contributions to \bar{Y} , respectively, and $\bar{Y}_t/\bar{Y}_u \propto \alpha$. Indeed, in the collisionally thin limit, where $\bar{Y} \propto \langle \ell \rangle$, an 84-fold increase in \bar{Y} occurs in Fig. 1(a), where $A = 80$. Additional enhancement of \bar{Y} can occur in the intermediate $\rho_d R$ range, where trapped tritons slow more effectively and sample the resonance peak in σ_{DT} .

Figure 1(a) shows $\bar{Y}_{meas} = (2.8 \pm 1.5) \times 10^{-2}$, observed on the highest yield MagLIF experiment to date [17], and the numerically calculated \bar{Y}_{num} for the experimentally

inferred parameters described above. Uncertainty estimates for \bar{Y}_{num} were obtained by varying the model inputs one at a time according to their associated experimental measurement uncertainties and summing up the relative deviations of \bar{Y}_{num} from the base case in quadrature. These uncertainties include $1 \lesssim \rho_d R \lesssim 3$ mg/cm², $2 \lesssim Z \lesssim 6$ mm, $2.6 \lesssim T_e \lesssim 3.8$ keV, $1 \lesssim$ burn time $\lesssim 2.5$ ns, and $0 \lesssim c_{Be} \lesssim 0.15$, where c_{Be} is the beryllium atom fraction mixed homogeneously into the hot spot.

A plausible upper limit on BR assumes perfect flux compression at the experimentally inferred stagnation radius, constrained by self-emission imaging [17]. For experimental $R_0 = 2.325$ mm and $B_0 = 10^5$ G, $R = 50$ μ m corresponds to a convergence ratio, $C_R \equiv R_0/R \approx 47$. Perfect flux conservation gives $(BR)_{id} = C_R(BR)_0 \approx 1.1 \times 10^6$ G cm. Areas in Fig. 1 where the red and blue regions overlap, with $BR \leq (BR)_{id}$, comprise the most likely average stagnation conditions.

The saturation of \bar{Y} at high BR implies that \bar{Y} primarily sets a lower limit on the fuel magnetization, $(BR)_h \gtrsim 4.5 \times 10^5$ G cm in this case, suggesting $(B)_h \gtrsim 90$ MG, with magnetic flux losses from the hot spot $\lesssim 60\%$, in reasonable agreement with integrated simulations [13,16]. (The subscript h is intended to remind the reader that we have mapped the true fuel conditions onto a homogeneous cylindrical column consistent with experimental observations. Effects associated with fuel nonuniformities will be described in a future publication and is beyond the scope of the present work.) For reference, $BR = 5 \times 10^5$ G cm corresponds roughly to $R/r_{L,t} \approx 2$. Thus, the measured \bar{Y} are unambiguously consistent with magnetically confined tritons. For comparison, an unrealistically optimistic convergence ratio, $C_R = 100$, with no axial fuel losses gives $\rho_d R \approx 15$ mg/cm², producing $\bar{Y} \lesssim 4 \times 10^{-3}$ at $T = 3.1$ keV and $BR < 10^5$ G cm, implying that fuel areal density alone cannot explain the observed \bar{Y} .

Neutron spectra.—Additional evidence of strong magnetization can be inferred from the DT neutron spectra, illustrated in Fig. 2. Figure 2(b) shows the measured DT neutron spectra viewed axially and radially from the best-performing MagLIF shot. The asymmetry is obvious, with the axial view indicating two peaks and having a broader full width than the radial view. Calculations of the DT spectrum from both views show good qualitative agreement with these features. The axially viewed spectra, all normalized to their peak values, are shown in Fig. 2(a) for three different values of stagnation BR , with plasma conditions consistent with the $\rho_d R = 2$ mg/cm² curve in Fig. 1(a). The radial view is shown in Fig. 2(c). The spectra are very sensitive to the level of magnetization, with the double-peak structure diminishing as the magnetic field increases, eventually becoming symmetric with the radial view. The radial view broadens substantially as BR increases. Within the uncertainties of the measured stagnation parameters, BR is the only parameter that has a significant effect on the spectra shape.

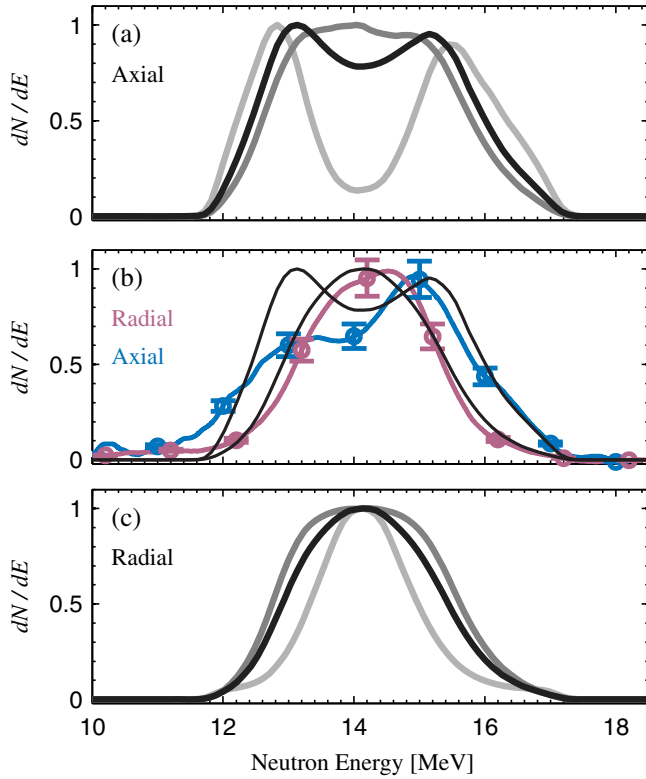


FIG. 2 (color online). (a) DT neutron spectra viewed axially calculated using $BR = 2.5 \times 10^5$ G cm (light gray curve), 4.2×10^5 G cm (black curve), and 7.0×10^5 G cm (gray curve). (b) Axially (blue) and radially (magenta) viewed DT neutron spectra from the recent MagLIF experiments, with representative error bars shown. (c) DT neutron spectra viewed radially calculated using the same values of BR as in (a). Black curves from (a) and (c) are overlaid on (b) for comparison.

The asymmetry is a consequence of the cylindrical geometry. At low magnetization, the tritons with the longest path length, and therefore the largest probability of reaction, are those with axially-directed velocities. This gives rise to a Doppler splitting (one peak for forward-directed and another for backward-directed tritons) in the axially-viewed neutron spectrum. Tritons moving perpendicular to the axis have a low probability of reaction, leaving the dip in the center of the axially-viewed spectrum. When viewed radially, the predominantly axially-directed reacting tritons produce no Doppler shift, giving rise to the single peak at 14.1 MeV. As the magnetic field increases, more tritons are confined radially with a resultantly wider distribution of axial velocities, which tends to merge the two Doppler peaks in the axially-viewed spectrum and smear out the dip in the middle. Peak magnetization causes most tritons to thermalize along confined trajectories regardless of their initial velocity orientation, creating symmetric spectra.

Comparison of the calculated and measured spectra suggests that the stagnation $BR \approx (4.2 \pm 0.5) \times 10^5$ G cm, slightly lower than the interval set by \bar{Y} . While beyond the scope of this study, preliminary analysis of isobaric,

radially-varying fuel profiles suggests that a cold, dense fuel layer near the liner tends to displace the entire $\bar{Y}(BR)$ curve upward by $O(10\%)$ without changing the threshold behavior significantly, which could bring the two methods into better agreement in future analyses. The left-right asymmetry in the measured axially-viewed spectrum could be due to axial fuel inhomogeneities, an azimuthal component in the compressed magnetic field, or other fuel attributes not accounted for in this analysis that could lead to (a) anisotropy in the triton velocity distribution function and/or (b) anisotropic \mathcal{R}_i for any single triton based on its birth velocity orientation.

Understanding mix with the DT:DD ratio.—The addition of a high- Z , nonreacting ion species into the fuel increases the effective ρR for triton stopping due primarily to enhanced electron drag [35]. Near the collisionally thin limit, a modest increase in \bar{Y} occurs with mix, since σ_{DT} increases as the triton slows [24,25]. One might suspect, then, based on Fig. 1, that failing to account for mix could lead to an overestimate of BR by underestimating $\bar{Y}(BR)$ for a given ρ_d . However, in the magnetized limit at moderate fuel densities, adding mix actually can decrease \bar{Y} and increase the inferred BR .

Figure 3 illustrates the dependence of \bar{Y} on $c_{Be} = n_{Be}/n$ under MagLIF-relevant conditions, where n_{Be} and n are the beryllium and total ion number densities, respectively. The beryllium is assumed to be fully ionized and mixed into the fuel homogeneously, both for simplicity and as a worst-case mix scenario. In the magnetized limit, the axial areal density of the deuterium, $\rho_d Z \approx 200$ mg/cm², is sufficient to thermalize most radially confined tritons, such that their average range $\langle \ell \rangle_{no\ mix} < Z$. Adding impurities decreases

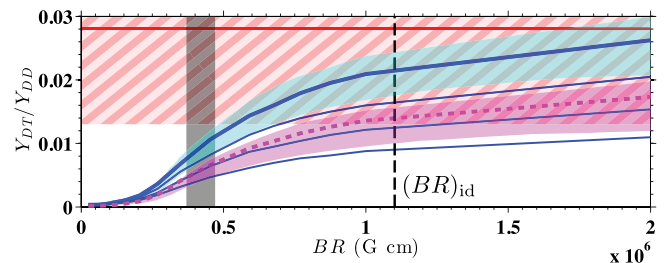


FIG. 3 (color online). DT:DD yield ratio versus BR and uniform beryllium mix for $\rho_d R = 2$ mg/cm² (solid blue lines) and $\rho_d R = 1$ mg/cm² (dashed magenta line). All other parameters same as solid blue curve in Fig. 1. Beryllium concentrations are (in ascending order) $c_{Be} = 0.3, 0.2, 0.1$, and 0 for $\rho_d R = 2$ mg/cm², and $c_{Be} = 0.1$ for $\rho_d R = 1$ mg/cm². Red line and hatched red area denote experimentally observed $\bar{Y}_{meas} = (2.8 \pm 1.5) \times 10^{-2}$ [17]. $(BR)_{id}$ corresponds to BR obtained by perfect flux compression (vertical dashed line). Vertical gray region indicates BR range estimated from neutron spectra (Fig. 2). The dashed magenta and thick solid blue lines correspond to two probable sets of conditions (with and without mix, respectively) as determined by independent emission analysis [17], and colored confidence intervals for those two curves are shown.

$\langle \ell \rangle$ further, with no compensating increase in ρ_d , hence reducing \bar{Y} . Thus, in the magnetized limit, adding mix increases the BR needed to explain a measurement of \bar{Y} at fixed $\rho_d R$.

At higher BR , \bar{Y} becomes less sensitive to variations in BR and increasingly sensitive to mix. In Fig. 3, only sufficiently small c_{Be} give \bar{Y} curves consistent with experimental observations, subject to the constraint $BR \lesssim (BR)_{id}$. Therefore, \bar{Y} sets an upper limit on the amount of (volumetric) mix at burn time. For the first MagLIF experiments, Fig. 3 suggests c_{Be} is most likely less than 10% in the burning fuel, with an upper bound of $\approx 20\%$. Separate analysis of emission and burn time measurements [17] gives the parameters associated with the two thicker curves in Fig. 3 as the most likely fuel conditions (with and without mix), also suggesting small mix fractions during burn ($< 10\%$), consistent with our estimate.

Discussion.—In this Letter, we have demonstrated the use of nuclear diagnostics to make critical determinations of fuel magnetization during burn in MIF. Magnetization of fast tritons also indicates magnetization of fuel electrons, since $\omega_{ct}\tau_{te} \approx \omega_{ce}\tau_{ee}$, where $\omega_{ct,ce}$ are the triton and electron gyrofrequencies, τ_{te} is the triton-electron slowing down time, and τ_{ee} is the electron-electron scattering time [35]. Since magnetic thermal insulation of the fuel is vital in MIF [10–17], understanding fuel magnetization and flux losses at stagnation could constrain the level of electron magnetization during implosion.

Successful triton confinement has direct implications for ignition-relevant MIF concepts employing DT fuel. In DT fusion, 3.5 MeV α -particles are emitted, whose magnetization is closely related to that of DD tritons: $\omega_{ca}\tau_{ae} \approx (1/2)\omega_{ct}\tau_{te}$. Also, DD tritons possess nearly identical birth gyroradii compared to DT α -particles: $r_{L,\alpha} \approx 1.07r_{L,t}$. Thus, the trapped α -particle fraction, $F_\alpha(BR)$, is quantitatively similar to $F_t(BR)$ [cf. Eq. (2)], and a platform that confines DD tritons will confine DT α -particles nearly as well. In MagLIF-relevant plasmas, the fraction of triton energy deposited into the fuel scales like the trapped triton fraction, $F_t = 25\%–70\%$ (cf. Fig. 1). Since the stopping length for $E_\alpha = 3.5$ MeV α -particles, $\ell_\alpha \propto (E_\alpha m_\alpha)^{1/2}/Z_\alpha^2$ [35], is approximately half that of 1.01 MeV tritons, the fraction of α -particle energy deposited in an analogous mixture of burning DT fuel would be comparable to or even exceed the fraction of triton energy deposited into the pure deuterium fuel. Reference [10] states that volume ignition in cylindrical, magnetized DT fuel requires $T = 7–10$ keV and $BR \geq (6.5–4.5) \times 10^5$ Gcm. Although the highest yield MagLIF experiment to date produced $T_e \approx 3.1$ keV, our analysis indicates $BR \gtrsim 4.5 \times 10^5$ Gcm is attainable, confirming that present MagLIF experiments are exploring a regime relevant to eventual ignition-scale ICF.

The authors gratefully acknowledge Mike Desjarlais, Kim Molvig, and Brian Appelbe for many useful discussions. This research was supported in part by an appointment to the Sandia National Laboratories Truman Fellowship in National Security Science and Engineering, which is part of the Laboratory Directed Research and Development (LDRD) Program, Project No. 165746, and sponsored by Sandia Corporation (a wholly owned subsidiary of Lockheed Martin Corporation) as Operator of Sandia National Laboratories under its U.S. Department of Energy Contract No. DE-AC04-94AL85000.

-
- [1] M. A. Sweeney and A. V. Farnsworth, Jr., *Nucl. Fusion* **21**, 41 (1981).
 - [2] I. R. Lindemuth and R. C. Kirkpatrick, *Nucl. Fusion* **23**, 263 (1983).
 - [3] R. D. Jones and W. C. Mead, *Nucl. Fusion* **26**, 127 (1986).
 - [4] A. Hasegawa, H. Daido, M. Fujita, K. Mima, M. Murakami, S. Nakai, K. Nishihara, K. Terai, and C. Yamanaka, *Phys. Rev. Lett.* **56**, 139 (1986).
 - [5] R. C. Kirkpatrick, I. R. Lindemuth, and M. S. Ward, *Fusion Technol.* **27**, 201 (1995), and references therein.
 - [6] J. H. Degnan *et al.*, *Phys. Rev. Lett.* **82**, 2681 (1999).
 - [7] R. E. Siemon, I. R. Lindemuth, and K. F. Shoenberg, *Comments Plasma Phys. Control. Fusion* **18**, 363 (1999).
 - [8] D. D. Ryutov and R. E. Siemon, *Comments Plasma Phys. Control. Fusion* **20**, 185 (2001).
 - [9] T. P. Intrator, J. Y. Park, J. H. Degnan, I. Furno, C. Grabowski, S. C. Hsu, E. L. Ruden, P. G. Sanchez, J. M. Taccetti, M. Tuszewski, W. J. Waganaar, G. A. Wurden, S. Y. Zhang, and Z. Wang, *IEEE Trans. Plasma Sci.* **32**, 152 (2004).
 - [10] M. M. Basko, A. J. Kemp, and J. Meyer-ter-Vehn, *Nucl. Fusion* **40**, 59 (2000).
 - [11] A. J. Kemp, M. M. Basko, and J. Meyer-ter-Vehn, *Nucl. Fusion* **41**, 235 (2001).
 - [12] A. J. Kemp, M. M. Basko, and J. Meyer-ter-Vehn, *Nucl. Fusion* **43**, 16 (2003).
 - [13] S. A. Slutz, M. C. Herrmann, R. A. Vesey, A. B. Sefkow, D. B. Sinars, D. C. Rovang, K. J. Peterson, and M. E. Cuneo, *Phys. Plasmas* **17**, 056303 (2010).
 - [14] S. A. Slutz and R. A. Vesey, *Phys. Rev. Lett.* **108**, 025003 (2012).
 - [15] M. E. Cuneo *et al.*, *IEEE Trans. Plasma Sci.* **40**, 3222 (2012).
 - [16] A. B. Sefkow, S. A. Slutz, J. M. Koning, M. M. Marinak, K. J. Peterson, D. B. Sinars, and R. A. Vesey, *Phys. Plasmas* **21**, 072711 (2014).
 - [17] M. R. Gomez *et al.*, preceding Letter, *Phys. Rev. Lett.* **113**, 155003 (2014).
 - [18] P. Y. Chang, G. Fiksel, M. Hohenberger, J. P. Knauer, R. Betti, F. J. Marshall, D. D. Meyerhofer, F. H. Séguin, and R. D. Petrasso, *Phys. Rev. Lett.* **107**, 035006 (2011).
 - [19] M. Hohenberger, P.-Y. Chang, G. Fiksel, J. P. Knauer, R. Betti, F. J. Marshall, D. D. Meyerhofer, F. H. Séguin, and R. D. Petrasso, *Phys. Plasmas* **19**, 056306 (2012).
 - [20] L. J. Perkins, B. G. Logan, G. B. Zimmerman, and C. J. Werner, *Phys. Plasmas* **20**, 072708 (2013).
 - [21] J. R. Rygg, F. H. Séguin, C. K. Li, J. A. Fringe, M. J.-E. Manuel, R. D. Petrasso, R. Betti, J. A. Delettrez,

- O. V. Gotchev, J. P. Knauer, D. D. Meyerhofer, F. J. Marshall, C. Stoeckl, and W. Theobald, *Science* **319**, 1223 (2008).
- [22] C. K. Li, F. H. Séguin, J. R. Rygg, J. A. Frenje, M. Manuel, R. D. Petrasso, R. Betti, J. Delettrez, J. P. Knauer, F. Marshall, D. D. Meyerhofer, D. Shvarts, V. A. Smalyuk, C. Stoeckl, O. L. Landen, R. P. J. Town, C. A. Back, and J. D. Kilkenny, *Phys. Rev. Lett.* **100**, 225001 (2008).
- [23] C. K. Li, F. H. Séguin, J. A. Frenje, M. Rosenberg, R. D. Petrasso, P. A. Amendt, J. A. Koch, O. L. Landen, H. S. Park, H. F. Robey, R. P. J. Town, A. Casner, F. Philippe, R. Betti, J. P. Knauer, D. D. Meyerhofer, C. A. Back, J. D. Kilkenny, and A. Nikroo, *Science* **327**, 1231 (2010).
- [24] H. Azechi, R. O. Stapf, N. Miyanaga, R. Tsuji, M. Yamanaka, S. Ido, K. Nishihara, T. Yabe, and C. Yamanaka, *Phys. Rev. Lett.* **59**, 2635 (1987).
- [25] S. Kurebayashi, J. A. Frenje, F. H. Séguin, J. R. Rygg, C. K. Li, R. D. Petrasso, V. Yu. Glebov, J. A. Delettrez, T. C. Sangster, D. D. Meyerhofer, C. Stoeckl, J. M. Soures, P. A. Amendt, S. P. Hatchett, and R. E. Turner, *Phys. Plasmas* **12**, 032703 (2005).
- [26] H.-S. Bosch and G. M. Hale, *Nucl. Fusion* **32**, 611 (1992).
- [27] M. D. Cable and S. P. Hatchett, *J. Appl. Phys.* **62**, 2233 (1987), and references therein.
- [28] Y. Setsuhara, H. Azechi, N. Miyanaga, H. Furukawa, R. Ishizaki, K. Nishihara, M. Katayama, A. Nishiguchi, K. Mima, and S. Nakai, *Laser Part. Beams* **8**, 609 (1990).
- [29] H. Azechi, M. D. Cable, and R. O. Stapf, *Laser Part. Beams* **9**, 119 (1991).
- [30] C.-K. Li and R. D. Petrasso, *Phys. Rev. Lett.* **70**, 3059 (1993).
- [31] J. S. Brzosko, J. R. Brzosko, Jr., B. V. Robouch, and L. Ingrosso, *Phys. Plasmas* **2**, 1259 (1995).
- [32] P. F. Schmit, K. Molvig, and C. W. Nakhleh, *Phys. Plasmas* **20**, 112705 (2013).
- [33] P. F. Knapp, D. B. Sinars, and K. D. Hahn, *Phys. Plasmas* **20**, 062701 (2013).
- [34] H. Brysk, *Plasma Phys.* **15**, 611 (1973).
- [35] P. Helander and D. J. Sigmar, *Collisional Transport in Magnetized Plasmas* (Cambridge University Press, New York, 2002).